nature structural & molecular biology

Stapled HIV-1 peptides recapitulate antigenic structures and engage broadly neutralizing antibodies

Gregory H Bird[1–3,8], Adriana Irimia[4–6,8], Gilad Ofek[7], Peter D Kwong[7], Ian A Wilson[4–6] & Loren D Walensky[1–3]

Hydrocarbon stapling can restore bioactive α-helical structure to natural peptides, yielding research tools and prototype therapeutics to dissect and target protein interactions. Here we explore the capacity of peptide stapling to generate high-fidelity, protease-resistant mimics of antigenic structures for vaccine development. HIV-1 has been refractory to vaccine technologies thus far, although select human antibodies can broadly neutralize HIV-1 by targeting sequences of the gp41 juxtamembrane fusion apparatus. To develop candidate HIV-1 immunogens, we generated and characterized stabilized α-helices of the membrane-proximal external region (SAH-MPER) of gp41. SAH-MPER peptides were remarkably protease resistant and bound to the broadly neutralizing 4E10 and 10E8 antibodies with high affinity, recapitulating the structure of the MPER epitope when differentially engaged by the two anti-HIV Fabs. Thus, stapled peptides may provide a new opportunity to develop chemically stabilized antigens for vaccination.

Antibodies neutralize pathogens by recognizing discrete and distinguishing peptidic motifs. By presenting primary, secondary and tertiary structures to the host immune system, vaccines have revolutionized the capacity to prevent human infection. Nevertheless, some targets, such as HIV type 1 (HIV-1), have been refractory to vaccine development. To achieve sterilizing HIV-1 immunity, an effective vaccine must elicit broadly neutralizing antibodies that intercept the virus before immune-cell penetrance[1]. Upon interaction of the HIV-1 envelope (Env) glycoprotein with host receptors, the Env viral fusion protein undergoes a series of conformational changes that are essential to penetrating the plasma membrane and fusing the viral and host membranes. Three copies of the HIV-1 envelope glycoproteins gp120 and gp41, which are noncovalently associated, form the Env trimer[2]. Once gp120 binds to CD4 (ref. 3) and co-receptor[4] on the host's cell membrane, gp41 transforms from its metastable native state into a fusogenic six-helix bundle[5,6] that conjoins viral and host-cell membranes, enabling viral-particle uptake. The regions of gp41 involved in this structural reorganization are the N-terminal heptad repeat (HR1) found just downstream of the fusion peptide and the C-terminal heptad repeat (HR2), which is close to the transmembrane region. The membrane-proximal external region[7] (MPER) is downstream from HR2 and contains antigenic sequences recognized by several broadly neutralizing human antibodies, including 2F5 (ref. 7), Z13e1 (ref. 8), 4E10 (ref. 9) and 10E8 (ref. 10).

Structural studies have identified critical motifs in gp41 that engage broadly neutralizing antibodies[10–17]. The crystal structure of 4E10 Fab in complex with a 13-residue portion of the MPER (amino acids 671–683) previously demonstrated that this peptide epitope adopts an α-helical conformation. Residues W672–D674 are configured as a short 3_{10} helix that directs the N terminus out of the binding site[18], and the interaction surface is composed of key residues W672, F673, I675 and T676 (ref. 12). Analysis of a longer 22-residue MPER peptide (amino acids 662–683) in a lipid context, by a combination of NMR and EPR spectroscopy, revealed a unique L-shaped structure reflecting a bipartite α-helix segmented by a kink[17]. The 10E8 antibody also recognizes an extended MPER peptide (amino acids 656–683) in a helix-kink-helix conformation, with each α-helix oriented 100° relative to the other[10]. In contrast, 2F5 binds to its target MPER sequences in a largely extended conformation with a central β-turn[16]. Importantly, upstream α-helical HR2 sequences, the transmembrane domain, the trimeric nature of the viral spike and the plasma membrane itself may provide an important structural context that constrains and thereby helps define the neutralization-competent antigenic structure(s) of the MPER[19].

Diverse approaches have been applied to display the MPER domain for vaccine development, including computational design of epitope scaffolds[20–24], MPER grafting[25], use of chimeric viruses[26] and immunization with cells expressing the gp41 postfusion complex[27]. Despite these efforts, non-neutralizing responses are the norm[23–25]. The conformations and orientations of MPER sequences displayed on the surface of nanoparticles[28], rhinovirus[26] or human cells[27] may be distinct from the pathologic epitope *in vivo* or may elicit off-target immune responses to the scaffold itself. Peptidic approaches to MPER mimicry have also been unsuccessful to date, potentially owing to limitations in

[1]Department of Pediatric Oncology, Dana-Farber Cancer Institute, Boston, Massachusetts, USA. [2]Division of Hematology/Oncology, Boston Children's Hospital, Boston, Massachusetts, USA. [3]Department of Pediatrics, Harvard Medical School, Boston, Massachusetts, USA. [4]Department of Integrative Structural and Computational Biology, Scripps Research Institute, La Jolla, California, USA. [5]International AIDS Vaccine Initiative Neutralizing Antibody Center, Scripps Research Institute, La Jolla, California, USA. [6]Scripps Center for HIV/AIDS Vaccine Immunology and Immunogen Discovery, Scripps Research Institute, La Jolla, California, USA. [7]Vaccine Research Center, National Institutes of Allergy and Infectious Diseases, National Institutes of Health, Bethesda, Maryland, USA. [8]These authors contributed equally to this work. Correspondence should be addressed to L.D.W. (loren_walensky@dfci.harvard.edu).

Received 4 August; accepted 23 October; published online 24 November 2014; doi:10.1038/nsmb.2922

peptide size, stability and delivery, as documented for peptide vaccine studies in general[29–31].

Introduction of noncovalent or covalent constraints to stabilize variably structured MPER sequences of different length has enhanced binding to select broadly neutralizing antibodies but has not necessarily elicited a broadly neutralizing response[32,33]. These data suggest that perhaps an MPER motif of optimal size or structure in the appropriate context (such as the membrane environment) was not reproduced, or structural integrity was not maintained *in vivo* because of proteolysis. We have found for structured therapeutic peptides that noncovalently constrained constructs are rapidly proteolyzed[34], and covalently constrained peptides bearing labile cross-links (for example, disulfides and amides) are also vulnerable. Indeed, the structural lability of the Env trimer itself was recently shown to be a critical factor in eliciting non-neutralizing anti–HIV-1 antibodies[35]. Although broadly neutralizing antibodies that target the HIV-1 envelope are among the most protective for preventing HIV-1 transmission, the requisite set of immunogens to appropriately guide an effective immune response has been elusive to date[36].

Two of the historically most broadly neutralizing monoclonal antibodies, 2F5 and 4E10, have been proposed to cross-react with self-antigens[37–42], thus raising the specter of autoreactivity as an unwanted consequence of a potential MPER-based vaccine. To preclude autoreactivity, a normal immune response may not permit the emergence of MPER-directed neutralizing antibodies. Such concerns, however, have been mitigated by the recent discovery of 10E8, a potent and broadly neutralizing antibody that also engages a helical MPER but does so without autoantigen recognition[10], thus providing a compelling basis for revisiting an MPER-based vaccine strategy. Interestingly, a recent follow-up study demonstrated that 10E8 retains weak affinity for lipid membranes and suggested a functional role for apical residues of its complementarity-determining region (CDR)-H3 in membrane binding and viral neutralization[43], as also observed for 2F5 (ref. 21) and 4E10 (ref. 20). When taken together, these studies indicate that effective HIV-1 neutralization by MPER-specific antibodies mechanistically involves interactions with viral lipids[16,20,21,43], yet structural delineation of the lipid-binding site(s) on MPER antibodies is lacking. Ultimately, structured MPER peptides presented in a lipid context or MPER-based antigens designed to contain lipid-recognition moieties may be ideally suited for vaccine development[43].

Motivated by fresh insights into the conformation of MPER epitopes in the membrane context[17] and in complex with potent and broadly neutralizing antibodies[10], we sought to design SAH-MPERs that reflect the full-length domain and reinforce both helical components of the helix-kink-helix structure. Our peptide-stapling method has yielded remarkably protease-resistant α-helical peptides[34], transforming tool reagents into prototype therapeutics with *in vivo* efficacy[44–47]. Importantly, the all-hydrocarbon constraint is itself protease resistant, thus differentiating this chemical approach from prior peptide-stabilization efforts and potentially rendering it well suited for the development of structured antigens in general. Here, we demonstrate that SAH-MPER peptides retain high-affinity binding activity toward two broadly neutralizing anti–HIV-1 antibodies, exhibit markedly enhanced protease resistance and recapitulate the critical antibody-recognition motif, as evidenced by crystal structures of the corresponding 4E10 and 10E8 complexes.

RESULTS

Design and 4E10-binding activity of SAH-MPER peptides

To generate candidate HIV-1 immunogens with neutralization-competent structure, we sought to replicate the bipartite α-helical conformation of the full-length MPER domain (**Fig. 1a**). To independently stabilize the respective N-terminal (662–671) and C-terminal (675–683) helices, which are separated by a flexible hinge region (672–674), we performed staple scans in each region of the MPER peptide. We substituted pairs of (*S*)-2-(((9H-fluoren-9-yl)methoxy)carbonylamino)-2-methyl-hept-6-enoic acids (abbreviated as *S*5 residues) at the *i* and *i* + 4 positions within the N-terminal region and performed ruthenium-catalyzed ring-closing metathesis (RCM) to generate six single-stapled peptides, termed SAH-MPER$_{(662–683)}$ A–F (**Fig. 1b** and **Supplementary Table 1**). Within the C-terminal region, we made *i*, *i* + 4 and *i*, *i* + 3 substitutions in order to accommodate α- or 3_{10}-helical conformation, generating 13 single-stapled peptides, termed SAH-MPER$_{(662–683)}$ G–L (*i*, *i* + 4) and M-S (*i*, *i* + 3) (**Fig. 1c**). Of note, *i*, *i* + 3 hydrocarbon stapling of *S*5 residues required a prolonged reaction time at elevated temperature to achieve yields similar to those of the traditional *i*, *i* + 4 reaction, which is consistent with pentane interference from the resultant cross-link that drapes over the N-terminal α-methyl group[48].

We compared the binding activity of 4E10 antibody across our diverse hydrocarbon-stapled peptides by competitive enzyme-linked immunosorbent assay (ELISA), pitting the unmodified MPER peptide (amino acids 662–683) against fluorescein isothiocyanate (FITC)-labeled competitor constructs. Whereas the affinity-driving contacts of 4E10 are on the C-terminal half of the MPER peptide[12], we chose to incorporate N-terminal MPER sequence into our designs to maximize their potential immunogenic surface. Among the N-terminal *i*, *i* + 4 stapled constructs, all but the most C-terminal F staple was tolerated, results consistent with this N-terminal portion of the MPER domain lying outside the core 4E10-binding region and with staple encroachment on the kink region being disfavored (**Fig. 1b**). Among the C-terminal *i*, *i* + 4 and *i*, *i* + 3 stapled constructs, only two constructs showed 4E10 binding activity. In each case, the favorable staple localized to the noninteracting helical surface and centered around the highly conserved L679-W680 motif. The C-terminal *i*, *i* + 4 staple K conferred a three-fold improvement in 4E10 binding activity, whereas the *i*, *i* + 3 staple Q yielded a 60-fold enhancement (**Fig. 1c**). The exquisite sensitivity of 4E10 binding activity to staple location emphasizes the importance of staple scanning to identify insertion points that balance structural reinforcement and preservation of key residues and binding interfaces.

To reinforce both helical motifs that flank the kink and to maximize protease resistance[34], we sought to generate double-stapled peptides, combining the C-terminal *i*, *i* + 3 Q staple with those N-terminal staple positions that yielded similar or improved 4E10 binding activity (A–E). However, the designed (*i*, *i* + 4), (*i*, *i* + 3) MPER constructs either failed to metathesize or resulted in minimal yield even after prolonged reaction at elevated temperatures, which is consistent with the requirement for relatively extreme conditions to accomplish single *i*, *i* + 3 stapling with *S*5. These results compelled us to determine which alternative non-natural olefin-bearing amino acids would enable *i*, *i* + 3 stapling to proceed as smoothly as single and double *i*, *i* + 4 stapling with *S*5 (ref. 34).

Optimization of *i*, *i* + 3 stapling for SAH-MPER design

We tested the reactivity of an alternative stapling amino acid pair in order to optimize *i*, *i* + 3 stapling for SAH-MPER synthesis. For a simplified peptide template, we used the previously described 4E10-binding epitope that corresponds to the C-terminal half of the MPER domain, with an appended trio of lysines to enhance solubility[18] (hereafter referred to as MPER$_{(671–683KKK)}$). We installed *S*5 residues at positions 678 and 681 and exposed the resin-bound peptide to ruthenium-catalyzed RCM for 2 h at room temperature, with no observed metathesis (data not shown). Then we escalated

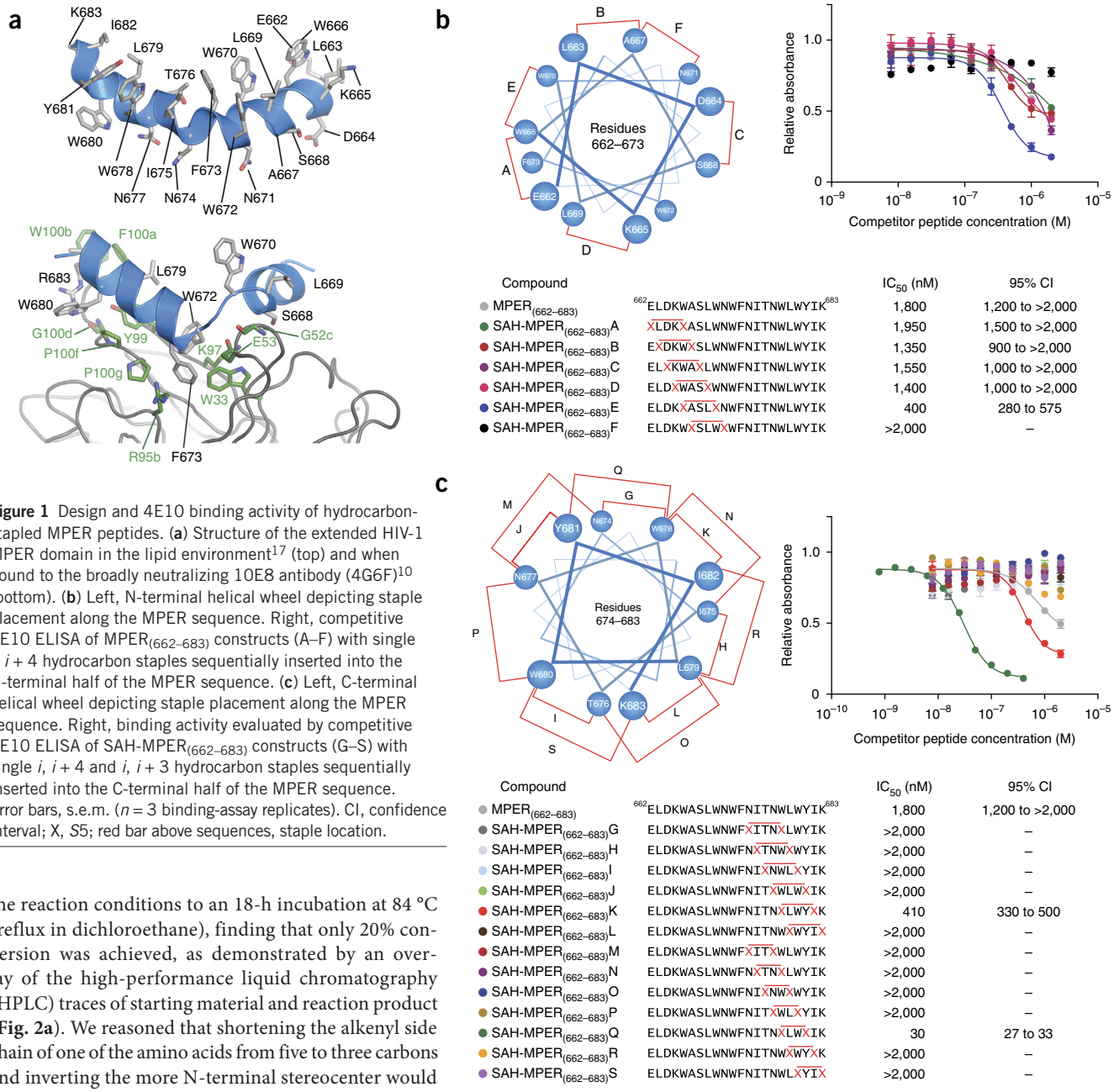

Compound		IC_{50} (nM)	95% CI
$MPER_{(662–683)}$	^{662}ELDKWASLWNWFNITNWLWYIK^{683}	1,800	1,200 to >2,000
SAH-$MPER_{(662–683)}$A	XLDKXASLWNWFNITNWLWYIK	1,950	1,500 to >2,000
SAH-$MPER_{(662–683)}$B	EXDKWXSLWNWFNITNWLWYIK	1,350	900 to >2,000
SAH-$MPER_{(662–683)}$C	ELXKWAXLWNWFNITNWLWYIK	1,550	1,000 to >2,000
SAH-$MPER_{(662–683)}$D	ELDXWASXWNWFNITNWLWYIK	1,400	1,000 to >2,000
SAH-$MPER_{(662–683)}$E	ELDKXASLXNWFNITNWLWYIK	400	280 to 575
SAH-$MPER_{(662–683)}$F	ELDKWXSLWXWFNITNWLWYIK	>2,000	–

Compound		IC_{50} (nM)	95% CI
$MPER_{(662–683)}$	^{662}ELDKWASLWNWFNITNWLWYIK^{683}	1,800	1,200 to >2,000
SAH-$MPER_{(662–683)}$G	ELDKWASLWNWFXITNXLWYIK	>2,000	–
SAH-$MPER_{(662–683)}$H	ELDKWASLWNWFNXTNWXWYIK	>2,000	–
SAH-$MPER_{(662–683)}$I	ELDKWASLWNWFNIXNWLXYIK	>2,000	–
SAH-$MPER_{(662–683)}$J	ELDKWASLWNWFNITXWLWXIK	>2,000	–
SAH-$MPER_{(662–683)}$K	ELDKWASLWNWFNITNXLWYXK	410	330 to 500
SAH-$MPER_{(662–683)}$L	ELDKWASLWNWFNITNWXWYIX	>2,000	–
SAH-$MPER_{(662–683)}$M	ELDKWASLWNWFXITXWLWYIK	>2,000	–
SAH-$MPER_{(662–683)}$N	ELDKWASLWNWFNXTNXLWYIK	>2,000	–
SAH-$MPER_{(662–683)}$O	ELDKWASLWNWFNIXNWXWYIK	>2,000	–
SAH-$MPER_{(662–683)}$P	ELDKWASLWNWFNITXWLXYIK	>2,000	–
SAH-$MPER_{(662–683)}$Q	ELDKWASLWNWFNITNXLWXIK	30	27 to 33
SAH-$MPER_{(662–683)}$R	ELDKWASLWNWFNITNWXWYXK	>2,000	–
SAH-$MPER_{(662–683)}$S	ELDKWASLWNWFNITNWLXYIX	>2,000	–

Figure 1 Design and 4E10 binding activity of hydrocarbon-stapled MPER peptides. (**a**) Structure of the extended HIV-1 MPER domain in the lipid environment[17] (top) and when bound to the broadly neutralizing 10E8 antibody (4G6F)[10] (bottom). (**b**) Left, N-terminal helical wheel depicting staple placement along the MPER sequence. Right, competitive 4E10 ELISA of $MPER_{(662–683)}$ constructs (A–F) with single *i*, *i* + 4 hydrocarbon staples sequentially inserted into the N-terminal half of the MPER sequence. (**c**) Left, C-terminal helical wheel depicting staple placement along the MPER sequence. Right, binding activity evaluated by competitive 4E10 ELISA of SAH-$MPER_{(662–683)}$ constructs (G–S) with single *i*, *i* + 4 and *i*, *i* + 3 hydrocarbon staples sequentially inserted into the C-terminal half of the MPER sequence. Error bars, s.e.m. (*n* = 3 binding-assay replicates). CI, confidence interval; X, *S5*; red bar above sequences, staple location.

the reaction conditions to an 18-h incubation at 84 °C (reflux in dichloroethane), finding that only 20% conversion was achieved, as demonstrated by an overlay of the high-performance liquid chromatography (HPLC) traces of starting material and reaction product (**Fig. 2a**). We reasoned that shortening the alkenyl side chain of one of the amino acids from five to three carbons and inverting the more N-terminal stereocenter would mitigate steric hindrance and orient the olefins toward each other. Therefore, we installed an *S5* residue at position 681 and an *R3* residue, (*R*)-2-(((9H-fluoren-9-yl)methoxy)carbonylamino)-2-methyl-pent-4-enoic acid, at position 678. Remarkably, we achieved almost complete conversion of the starting material into metathesized product with only 2 h incubation at room temperature, results matching the synthetic efficiency of *i*, *i* + 4 stapling with two *S5* residues (**Fig. 2b**). In accordance with the enhanced 4E10 binding affinity derived from *S5*-*S5* stapling at the Q position of the full-length MPER peptide, *R3*-*S5* stapling of the 671–683KKK construct at position Q (designated q to reflect the alternate staple composition) resulted in five-fold improvement in competitive binding activity compared to that of the unmodified $MPER_{(671–683KKK)}$ peptide (**Fig. 2c**).

Crystal structure of a stapled MPER peptide bound to 4E10

We determined the crystal structure of the 4E10 Fab–SAH-$MPER_{(671–683KKK)}$(q) complex at 2.9-Å resolution with one Fab–peptide complex per asymmetric unit (**Fig. 3a** and **Table 1**). With the exception of the C-terminal lysine side chains, all main chains and side chains of the stapled peptide residues could be modeled into the electron density map (**Fig. 3b**). The relatively weak electron density for the region of the six-atom carbon staple, which replaced the side chains of W678 and Y681, could not distinguish between *Z* and *E* olefin isomers (or exclude the possibility of a stereoisomeric mixture) and was modeled in a *Z* conformation in this 2.9-Å structure. Density appeared for most of the main chain of the flexible CDR-H3 loop (residues 99–100D, except $W100^{(H)}$ and $G100A^{(H)}$, where the (H) superscript stands for heavy chain) (**Supplementary Fig. 1a**)[18]. The complexes of 4E10 Fab with SAH-$MPER_{(671–683KKK)}$(q) and the original (unmodified) 4E10-epitope peptide (PDB 2FX7)[18] superpose with an r.m.s deviation of 0.73 Å for the Cα atoms and are overall very similar (**Supplementary Fig. 1b**). Superposing the peptide regions revealed essentially identical Fab-binding interfaces, highlighting that the q staple reinforces

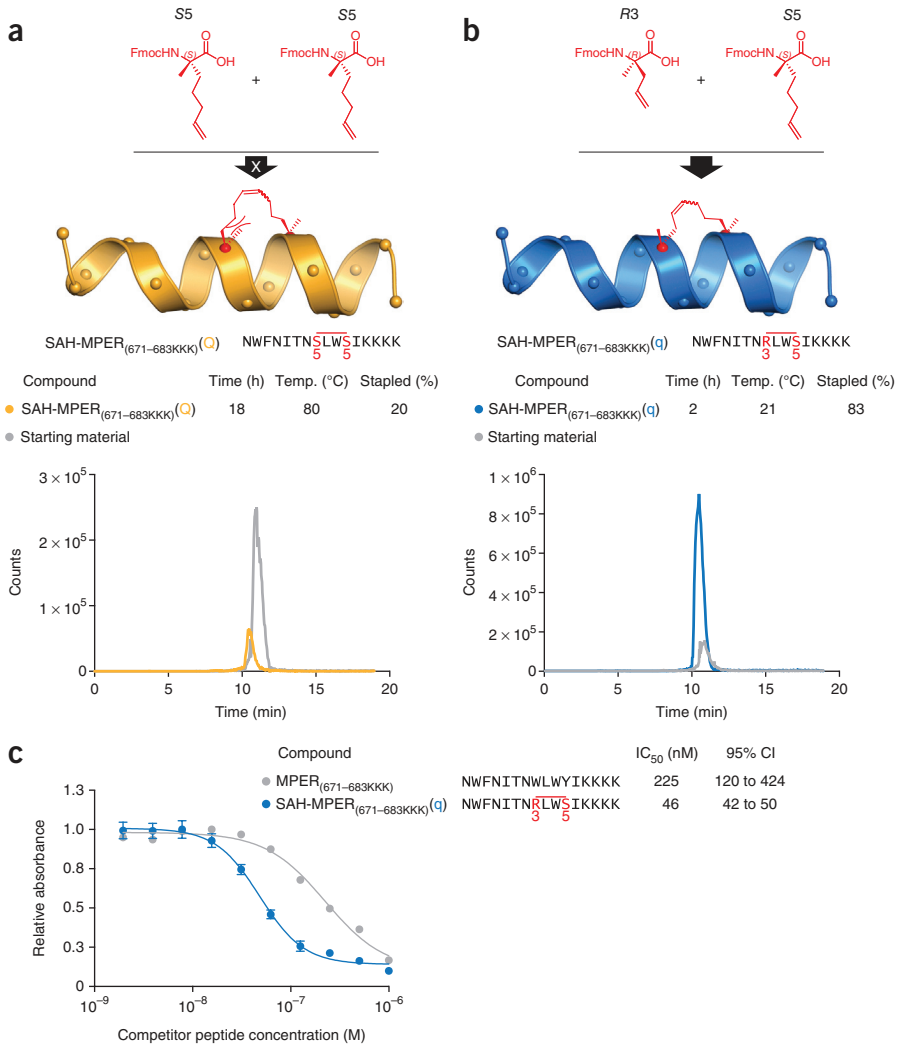

Figure 2 Chemical optimization of *i*, *i* + 3 hydrocarbon stapling. (**a**) Top, design and synthesis of SAH-MPER$_{(671–683KKK)}$(Q), using *S*5 olefinic tethers to generate the *i*, *i* + 3 staple. Bottom, HPLC traces of starting material (gray) and product (yellow), demonstrating the low yield of reaction product even after prolonged incubation at reflux conditions. (**b**) Top, design and synthesis of SAH-MPER$_{(671–683KKK)}$(q), in which the N-terminal *S*5 residue was replaced with *R*3 to lead to efficient *i*, *i* + 3 olefin metathesis under standard reaction conditions. Bottom, HPLC traces of starting material (gray) and product (blue), demonstrating the high yield of reaction product. (**c**) Competitive 4E10 binding activity of SAH-MPER$_{(671–683KKK)}$(q) compared to the corresponding unstapled peptide. Error bars, s.e.m. (n = 3 binding-assay replicates). Fmoc, fluorenylmethoxycarbonyl; CI, confidence interval; temp, temperature.

the natural peptide-bound structure (**Fig. 3c**). Like the side chains of W678 and Y681, the six-carbon staple that replaces these natural residues does not contact the antibody, owing to its location on the solvent-exposed face of the helical peptide. Thus, hydrocarbon stapling effectively recapitulates the native antigenic epitope, with the structurally reinforcing staple positioned away from, and thereby not perturbing, the critical binding interface.

Identification of a phosphate-binding site on 4E10

The MPER-specific antibodies 2F5 and 4E10 can also bind several phospholipid antigens[39]. The initial difference Fourier electron density map of our 4E10 Fab–SAH-MPER$_{(671–683KKK)}$(q) complex revealed roughly spherical electron density of approximately 7σ located between S28H and S30H of the CDR-H1 loop (**Fig. 4a**,**b**). Both phosphate and chloride ions were present in the crystallization conditions (based on mother-liquor conditions that contained sodium and potassium phosphate (0.1 M) and sodium chloride (0.2 M)). When a chloride ion was refined into the extra density, residual positive electron density still remained in $F_o - F_c$ maps. Thus, we interpreted the spherical density as a phosphate ion, which fits the density with a real-space correlation coefficient of 0.96. Although the *B* value for the phosphate ion is high (~110 Å^2, **Table 1**) compared to that of the overall protein, it is nevertheless close to that of neighboring CDR-H1 residues (~90 Å^2 for S28$^{(H)}$, 74 Å^2 for F29$^{(H)}$ and 83 Å^2 for S30$^{(H)}$; **Fig. 4b**). Elevated isotropic *B* values were also observed for these CDR-H1

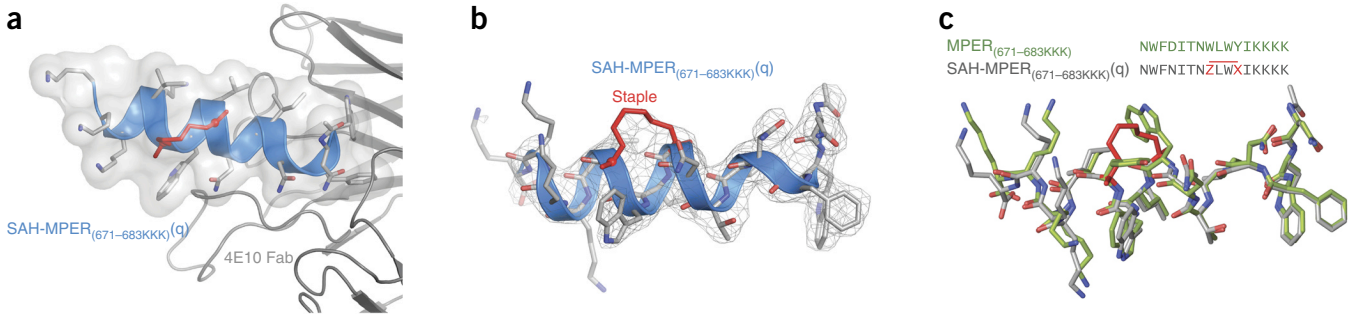

Figure 3 Structural analysis of the 4E10 Fab–SAH-MPER$_{(671–683KKK)}$(q) complex. (**a**) Crystal structure of SAH-MPER$_{(671–683KKK)}$(q) (shown as a blue ribbon and gray transparent van der Waals surface) bound to 4E10 Fab, at 2.9-Å resolution. (**b**) $2F_o - F_c$ electron density map (1σ level) of the antibody-bound SAH-MPER$_{(671–683KKK)}$(q) peptide. (**c**) Superposition of the native (green; PDB 2FX7)[18] and *i*, *i* + 3–stapled (gray) MPER$_{(671–683KKK)}$ peptides, highlighting the similarity of antibody-bound structures, aside from the appended C-terminal lysines and the incorporated staple. Z and X represent *R*3 and *S*5, respectively, in the staple (red bar above sequence).

Table 1 Data collection and refinement statistics

	4E10 Fab SAH-MPER$_{(671–683KKK)}$(q)	4E10 Fab SAH-MPER$_{(671–683KKK)}$(q)pSer	10E8 Fab SAH-MPER$_{(662–683KKK)}$(B,q)
Data collection			
Space group	$P6_122$	$P6_122$	$P2_12_12_1$
Cell dimensions			
a, *b*, *c* (Å)	226.10, 226.10, 41.82	226.51, 226.51, 42.33	68.6, 126.3, 129.9
α, β, γ (°)	90, 90, 120	90, 90, 120	90, 90, 90
Resolution (Å)[a]	48.95–2.91 (2.96–2.91)	49.04–2.68 (2.75–2.68)	50–4.15 (4.25–4.15)
R_{merge} (%)[b]	18.2 (66.6)	9.3 (59.7)	30.2 (56.4)
R_{pim}	4.2 (22.7)	2.1 (13.4)	
$I / \sigma I$	16.4 (3.1)	28.0 (5.6)	5.6 (2.9)
Completeness (%)	95.6 (70.4)	99.9 (100)	95.1 (83.3)
Redundancy	21.9 (7.8)	20.7 (20.3)	6.4 (5.1)
Refinement			
Resolution (Å)	48.95–2.91	49.04–2.68	40.05–4.20 (4.35–4.20)
No. reflections	13,737 (501)	18,583 (1,335)	8,120 (624)
R_{work} / R_{free} (%)	21.0 / 26.8	17.0 / 22.2	22.5 / 28.1
No. atoms			
Protein	3,353	3,344	7,020
Peptide	150	162	156
PO_4 ion	5	–	–
Trifluoroacetic acid	14	–	–
Water	29	98	–
B factors (Å^2)			
Wilson plot	63.8	52.0	71.0
Protein	70.7	51.2	92.6
Peptide	81.1	59.8	96.1
Staple	75.0	48.5	90.1
PO_4 ion	110.5	–	–
Dab-Gly-pSer	–	105.6	–
Water	50.5	46.7	–
r.m.s. deviations			
Bond lengths (Å)	0.006	0.010	0.002
Bond angles (°)	0.79	1.34	0.60

[a]Values in parentheses are for highest-resolution shell. [b]Data sets from two crystals were merged together for 4E10 Fab–SAH-MPER$_{(671–683KKK)}$(q). A full data set was collected on one crystal for 4E10 Fab–SAH-MPER$_{(671–683KKK)}$(q)pSer and for 10E8 Fab SAH-MPER$_{(662–683KKK)}$(B,q).

loop residues in the previous 4E10 Fab–native MPER$_{(671–683KKK)}$ (PDB 2FX7)[18] structure in comparison to mean isotropic and Wilson *B* values at the corresponding resolution[18], thus suggesting increased structural flexibility. The superposition of the phosphate-incorporated site with the same region in the 4E10 Fab–native MPER$_{(671–683KKK)}$ complex (PDB 2FX7)[18], which was crystallized from phosphate-free buffer, demonstrates torqueing of backbone amides and reorientation of the S28$^{(H)}$ hydroxyl toward the phosphate ion to promote favorable hydrogen-bond interactions in the 4E10 Fab–SAH-MPER$_{(671–683KKK)}$(q) structure (**Fig. 4c**). The presence of a phosphate-binding site in the CDR-H1 loop region of 4E10 is consistent with antibody binding to anionic lipids at the membrane surface. Indeed, the orientation of SAH-MPER$_{(671–683KKK)}$(q) within the antigen-binding site positions the C-terminal residues 684–686, which are replaced here by lysines and would compose the start of the gp41 transmembrane segment, immediately adjacent to the identified phosphate-binding site (**Fig. 4a**).

To our knowledge, we have detected this phosphate-binding site in the 4E10 combining region for the first time, because a PDB search of all available 4E10 structures did not reveal phosphate as a buffer component of prior crystallization conditions. A recent crystal structure of the 4E10 variable region (Fv) in a ligand-free form[49] shows sulfate ions near the CDR-H1 loop, but none of the ions are in the same position as that observed here for the phosphate. In fact, a glycerol molecule is present in this position in one of the four Fv molecules in the asymmetric unit. Whereas sulfate and phosphate ions are similar, and can occupy the same binding site in a protein, the peptide-free structure of 4E10 (ref. 49) has its CDR-H1 and CDR-H3 loops drastically perturbed in comparison to the peptide-bound form[18]. In the ligand-free structure, the CDR-H3 occupies the peptide-binding site but is also involved in extensive packing interactions with symmetry-related

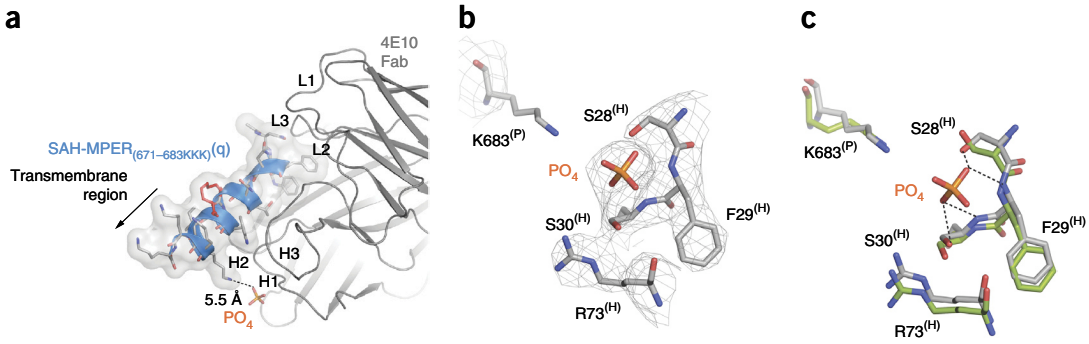

Figure 4 Identification of a candidate phospholipid-binding site at the 4E10 interface. (**a**) Incorporation of a phosphate ion from the mother liquor into the crystal structure of the 4E10 Fab–SAH-MPER$_{(671–683KKK)}$(q) complex. The presence of a phosphate-binding site in the CDR-H1 loop region of 4E10 is consistent with its binding mode at the membrane surface. The transmembrane region (replaced here by three lysines for solubility purposes) that would be membrane embedded in the virion is indicated with an arrow. (**b**) $2F_o - F_c$ electron density map (1σ level) of the phosphate-binding site located between residues S28$^{(H)}$ and S30$^{(H)}$ of the CDR-H1 loop. (**c**) Superposition of the phosphate-incorporated site of the 4E10 Fab–SAH-MPER$_{(671–683KKK)}$(q) structure (gray) with that region of the 4E10 Fab–native MPER$_{(671–683KKK)}$ peptide complex (green; PDB 2FX7[18]).

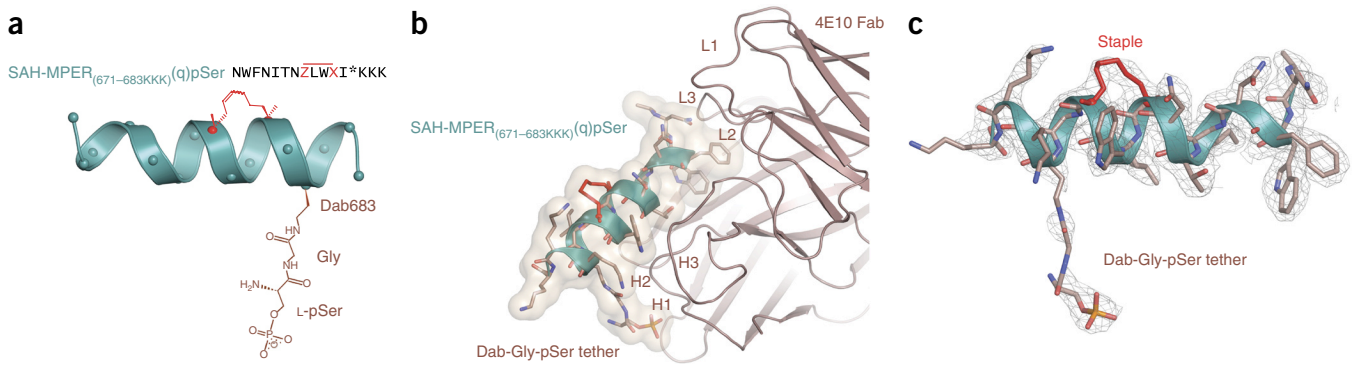

Figure 5 A phosphate tether incorporated into SAH-MPER$_{(671–683KKK)}$(q) engages the putative lipid-binding site. (**a**) Position 683 of SAH-MPER$_{(671–683KKK)}$(q) derivatized with a Dab-Gly-pSer tether (brown, and indicated by asterisk in sequence) to span the measured 5.5 Å between the primary amine of Lys683 and the phosphate observed at the 4E10 Fab–SAH-MPER$_{(671–683KKK)}$(q) interface. Z and X represent *R*3 and *S*5, respectively, in the staple (red bar above sequences). (**b**) Crystal structure of the SAH-MPER$_{(671–683KKK)}$(q)pSer complex (shown as a green ribbon and wheat transparent Van der Waals surface) bound to 4E10, at 2.68-Å resolution. (**c**) The $2F_o - F_c$ electron density map (1σ level) of the antibody-bound SAH-MPER$_{(671–683KKK)}$(q)pSer construct.

mates. It is also noteworthy that the acidic pH of 4.6 and the high salt concentration (0.4–0.8 M Li_2SO_4) in the crystals could affect the conformation. To avoid exposure of the hydrophobic residues in the combining site, which otherwise interacts with the MPER, the CDR-H3 loop forms extensive packing interactions with symmetry-related mates and residues of the peptide-binding site. Thus, the disposition of the phosphate ion reported here in the ligand-bound structure in the CDR-H1 of 4E10 could indeed reflect a 4E10 membrane-binding interface. That said, we do not exclude participation of the hydrophobic CDR-H3 in membrane lipid interactions, as reported for 2F5 (refs. 16,21), 4E10 (ref. 20) and 10E8 (ref. 43).

Crystal structure of 4E10 and a SAH-MPER phosphopeptide

To probe the potential role of phosphate engagement as a 4E10 binding determinant at the membrane, we generated a modified SAH-MPER$_{(671–683KKK)}$(q) peptide containing a tethered phosphate moiety. From the predicted 5.5-Å distance between the K683 side chain amine and phosphate group (**Fig. 4a**), we modeled in a phosphoserine (pSer) group and determined that it could be appropriately linked to the peptide backbone by a diaminobutanoic acid–glycine (Dab-Gly) spacer at position 683 (**Fig. 5a**). We then synthesized SAH-MPER$_{(671–683KKK)}$(q) containing the Dab-Gly-phosphoserine (pSer) tether at the 683 position or, as a negative control, at the 685 position, which would orient pSer away from the binding interface (**Supplementary Fig. 2a**). Competitive 4E10 binding analysis revealed a slight improvement in binding affinity upon incorporation of a phosphate moiety at position 683, whereas installing the equivalent derivatization at position 685 actually reduced binding activity (**Supplementary Fig. 2b**).

To confirm that the installed phosphate moiety at position 683 interacted with the defined phosphate-binding site at the 4E10 interface, we undertook structural analysis of the 4E10 Fab bound to phosphate-derivatized SAH-MPER$_{(671–683KKK)}$(q)pSer peptide containing the Dab-Gly spacer. We determined the structure of the complex at 2.68-Å resolution from a crystal grown in phosphate-free mother liquor (**Fig. 5b**). The initial difference Fourier map shows unambiguous positive electron density for the covalently linked staple, which fit the electron density with a real-space correlation coefficient of 0.98 and an isotropic *B* value of 49 Å^2, in good agreement with the Wilson plot and mean isotropic *B* values (**Table 1** and **Supplementary Fig. 3a**,**b**).

In contrast, the initial positive $F_o - F_c$ (3σ level) and the $2F_o - F_c$ (1σ level) maps show incomplete electron density for the central portion of the Dab-Gly linker (**Supplementary Fig. 4a**). However, the final $2F_o - F_c$ density of the Dab linker (**Supplementary Fig. 4b**) improved after refinement as compared to the density for the SAH-MPER$_{(671–683KKK)}$(q) K683 (**Fig. 4b**) or with the density for the same lysine in the 1.76-Å structure of native MPER$_{(671–683KKK)}$ in complex with 4E10 (PDB 2FX7)[18], where we observed density for only the main chain. With the exception of two atoms (OZ1 and N6), all of the atoms of the Dab-Gly-pSer are located inside the $2F_o - F_c$ electron density map at the 0.8σ level (**Supplementary Fig. 4c**). Therefore, the strong density (5σ level in the initial $F_o - F_c$ map) for the phosphate moiety and the improved density of the Dab linker, combined with the absence of phosphate in the mother liquor, indicate that the Dab-Gly-pSer tether at position 683 extends into the phosphate-binding site (**Fig. 5b**,**c** and **Supplementary Fig. 4d**). However, for the linker atoms that connect the peptide backbone to the phosphate moiety, we observed reduced density for the eight-atom linker and a high isotropic *B* value of approximately 112 Å^2 (~105 Å^2 for the whole Dab-Gly-pSer moiety; **Table 1**), indicative of its flexibility. The 4E10 Fab complexes with SAH-MPER$_{(671–683KKK)}$(q)pSer and SAH-MPER$_{(671–683KKK)}$(q) are otherwise very similar, with only 0.23-Å r.m.s. deviation (all Cα atoms) for the Fab and 0.17-Å r.m.s. deviation (all Cα atoms) for the corresponding peptides (**Supplementary Fig. 1b** and **Supplementary Fig. 3c**).

Potency and stability of double-stapled MPER epitopes

The small size of the MPER$_{(671–683KKK)}$ template and its limited sites for installing staples, along with its rapid proteolysis (**Supplementary Fig. 5**), continued to render (*i*, *i* + 4), (*i*, *i* + 3) double-stapling of the extended MPER peptide the most compelling design to maximize immunogenic surface, reinforce neutralization-competent structure and ensure protease resistance. Applying *R*3-*S*5 (*i*, *i* + 3) and *S*5-*S*5 (*i*, *i* + 4) stapling, we successfully generated all five double-stapled constructs with the standard 4-h, room-temperature metathesis conditions (**Fig. 6a**). Competitive 4E10 binding analysis demonstrated half-maximal inhibitory concentration (IC_{50}) values in the 130–600 nM range for double-stapled SAH-MPER$_{(662–683)}$ peptides. The best binder, SAH-MPER$_{(662–683)}$(D,q), nearly matched the binding activity of the corresponding single-stapled SAH-MPER$_{(662–683)}$(q) construct

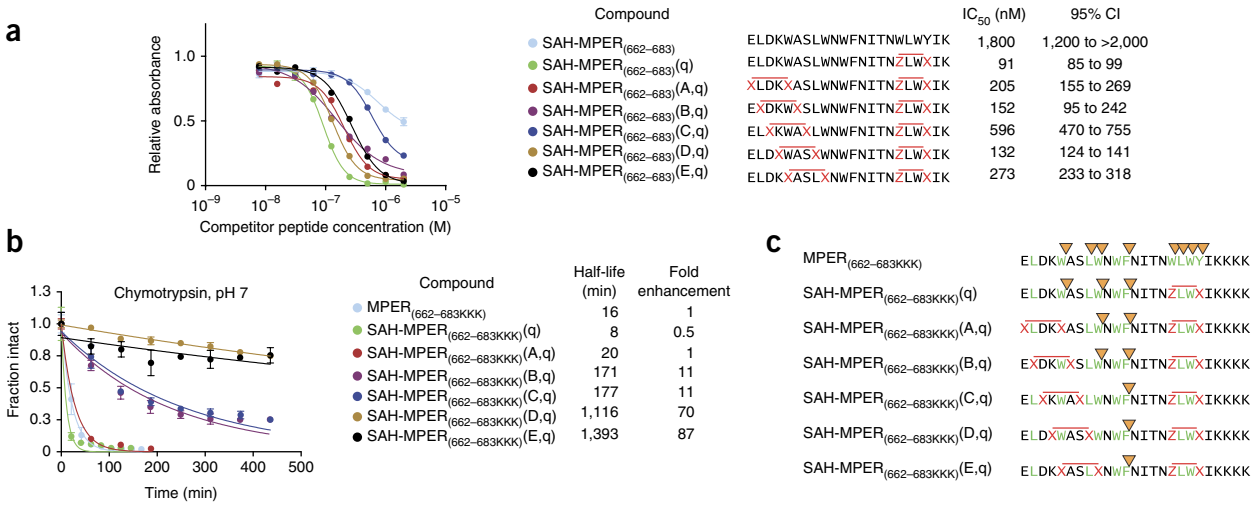

Figure 6 Synthesis, protease stability and 4E10 binding activity of double-stapled SAH-MPER peptides. (**a**) 4E10 binding activity of a series of double-stapled SAH-MPER$_{(662–683)}$ peptides, tested by competitive ELISA. (**b**) Comparative chymotrypsin resistance of SAH-MPER$_{(662–683)}$ peptides, as monitored by LC/MS over time. Proteolysis was performed with SAH-MPER constructs bearing C-terminal KKKs to optimize peptide ionization for MS analysis. Error bars, s.e.m. (n = 3 proteolysis-reaction replicates). (**c**) MS-based peptide-fragment analysis identifying the sites of chymotrypsin proteolysis. In comparison to the cleavage pattern of the unmodified MPER peptide, chymotrypsin sites (arrowheads) located within or adjacent to the installed staples (denoted by red bars and red X-X, Z-X pairs) were completely protected from proteolysis. The cleavage kinetics for intervening sites was progressively slowed (A,q<B,q<C,q<D,q<E,q) by the induced structure of the N-terminal staple as it moved stepwise in the C-terminal direction (red X-X pairs). CI, confidence interval; green residues, theoretical chymotrypsin sites; orange arrowheads, observed chymotrypsin cleavage.

(132 nM versus 91 nM, respectively), in which the 4E10-binding determinant (amino acids 671–683) is optimally stabilized by an i, i + 3 staple at positions 678 and 681 (**Fig. 6a**).

To interrogate the relative protease resistance of double-stapled SAH-MPER constructs, we subjected peptides to chymotrypsin proteolysis and monitored the time-dependent degradation of full-length SAH-MPER by HPLC-MS. Because the double-stapled SAH-MPER$_{(662–683)}$ constructs ionized poorly upon MS analysis, we also synthesized the library of constructs with C-terminal KKK tails; this increased ionization potential and facilitated detection of a greater breadth of fragment ions. As observed for the corresponding unmodified and q-stapled MPER$_{(671–683KKK)}$ constructs (**Supplementary Fig. 5**), the unmodified and q-stapled full-length MPER$_{(662–683KKK)}$ peptides showed similar rapid-proteolysis profiles (**Fig. 6b**). In contrast, the introduction of double staples into the MPER$_{(662–683KKK)}$ sequence prolonged the proteolytic half-life by approximately 10- to 90-fold compared to that of the corresponding unstapled construct (**Fig. 6b**). Of the eight chymotrypsin proteolysis sites observed for the unmodified peptide, the most stable double-stapled SAH-MPERs eliminated the capacity of chymotrypsin to cleave all but one of them (**Fig. 6c** and **Supplementary Fig. 6**). Indeed, those chymotrypsin sites flanked by staples or located immediately adjacent to staples were completely shielded from proteolysis (**Supplementary Fig. 6**). Thus, at the expense of only a minor decrease in binding activity relative to the single-stapled SAH-MPER$_{(662–683)}$(q) construct (1.4-fold), the double-stapled SAH-MPER$_{(662–683)}$(D,q) peptide, for example, achieves a 140-fold increase in chymotrypsin resistance. Although here we initially used 4E10 binding activity as a guide for candidate immunogen design, it is important to note that the variety of MPER-specific neutralizing antibodies identified to date recognize a spectrum of peptide templates and conformations. Thus, in addition to the 4E10-optimized double-stapled MPER peptides (**Fig. 6a**), constructs that do not engage 4E10 (**Fig. 1b**,**c**) could potentially represent a library of alternatively structured yet highly stable MPERs for immunization.

Engagement of double-stapled MPER peptides by 10E8

The recent discovery of the 10E8 broadly neutralizing HIV-1 antibody[10] provided a unique opportunity to explore the binding interactions between our double-stapled SAH-MPERs and a different anti-MPER Fab that recognizes a helically structured MPER. We performed a 10E8 competitive ELISA binding assay analogous to that described above for 4E10 and again identified a series of compounds with nanomolar Fab-binding activity, including SAH-MPER$_{(662–683)}$(A,q), SAH-MPER$_{(662–683)}$(B,q) and SAH-MPER$_{(662–683)}$(E,q) (**Fig. 7a**). Notably, SAH-MPER$_{(662–683)}$(C,q) and SAH-MPER$_{(662–683)}$(D,q), which bound to 4E10 Fab in the same nanomolar range as the other constructs (**Fig. 6a**), showed no binding activity to 10E8 Fab (**Fig. 7a**). These data are consistent with binding interactions between 10E8 and residues that localize to the N-terminal portion of the MPER epitope[10], such as S668 and L669, which are replaced by stapling amino acids in the (C,q)- and (D,q)-stapled MPER peptides. Although MPER residue W670 also contacts 10E8, replacement of this residue in SAH-MPER$_{(662–683)}$(E,q) by a staple spanning the W666–W670 positions preserved high-affinity 10E8 interaction. Thus, whereas 4E10 Fab sensed no differences in N-terminal staple position, due to Fab engagement of the C-terminal portion of the MPER domain only, the 10E8 Fab was more discriminating in the upstream region that included N-terminal residues of the MPER domain.

To determine whether hydrocarbon double-stapling maintained the 10E8-bound conformation of the MPER domain, we determined the crystal structure of the 10E8 Fab in complex with SAH-MPER$_{(662–683KKK)}$(B,q) (**Fig. 7b**). Crystals of the complex diffracted to 4.15-Å resolution (**Table 1**), and we solved the structure with molecular replacement and refined it to R_{work}/R_{free} of 22.5%/28.1%. Two complexes were present in the asymmetric unit, with their corresponding peptides displaying a Cα r.m.s. deviation of 0.3 Å across gp41 residues 670–683. We observed electron density around the C-terminal portion of the peptide, corresponding to gp41 residues S668–K683 for chain P (L669–K683 for chain C), which appeared to only partially cover the staple between residue positions 678 and 681 (**Supplementary Fig. 7a**).

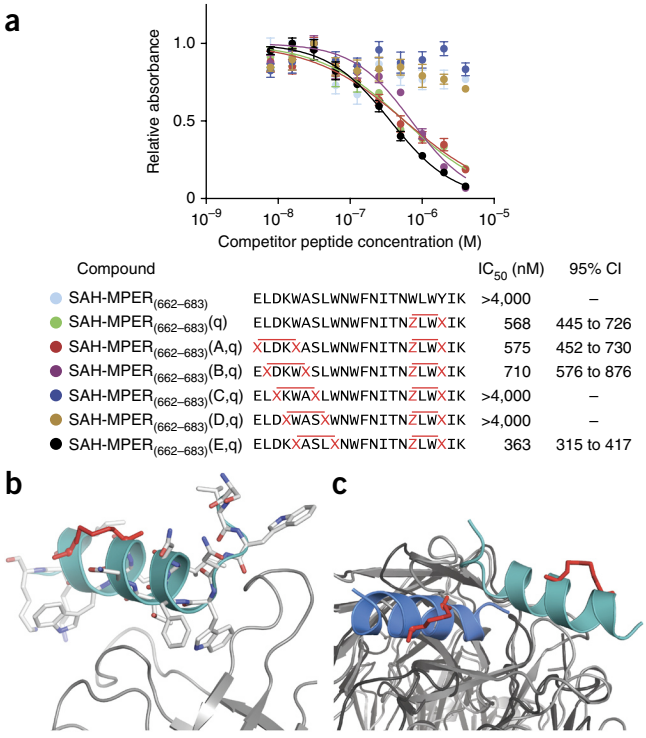

Figure 7 10E8 binding activity of double-stapled SAH-MPER peptides and structural analysis of the 10E8 Fab–SAH-MPER$_{(662–683KKK)}$(B,q) complex. (**a**) Comparative binding activity of double-stapled SAH-MPER$_{(662–683)}$ peptides for 10E8, as measured by competitive ELISA against the unmodified 10E8 ligand RRRNEQELLELDKW ASLWNWFDITNWLWYIRRRR[10]. (**b**) Crystal structure of SAH-MPER$_{(662–683KKK)}$(B,q) (shown as a cyan ribbon with stick residues) bound to 10E8 Fab at 4.15-Å resolution. (**c**) Superposition of the 4E10 Fab–SAH-MPER$_{(671–683KKK)}$(q) and 10E8 Fab–SAH-MPER$_{(662–683KKK)}$(B,q) complexes, highlighting how the two anti-HIV Fabs differentially engage the stapled MPER antigens.

The region upstream of chain-P residue S668 (or chain-C residue L669) that included the staple between positions 663 and 667 was disordered and could not be built. Nevertheless, the distinctive kink and adjacent N-terminal residues that distinguish 10E8 from 4E10 interactions with the MPER domain are visualized and recapitulated in the 10E8 Fab–SAH-MPER$_{(662–683KKK)}$(B,q) complex (**Fig. 7b**).

Overall, the structure revealed that the staple between residue positions 678 and 681 largely reinforced the helical conformation of the C-terminal portion of the MPER peptide, as observed in the structure of 10E8 bound to the native gp41 MPER[10]. We observed the highest degree of structural homology between the 10E8-bound stapled and unmodified peptides between residues 670 and 683, thus yielding Cα and all-atom r.m.s. deviations of 0.6 and 1.8 Å, respectively (**Supplementary Fig. 7b** and **Supplementary Table 2**). Comparison of the contact interfaces between 10E8 and the stapled and unmodified gp41 MPER peptides also revealed a high degree of similarity, with many of the same residues mediating the interactions between them (**Supplementary Table 3**). An interfacial surface area of 633 Å^2 was buried on the SAH-MPER$_{(662–683KKK)}$(B,q) peptide, and 713 Å^2 was buried on the antibody. The heavy chain of 10E8 accounted for a majority of the interactions with the double-stapled peptide, representing 92% of the interface, in agreement with the interactions observed between the 10E8 heavy chain and the native gp41 MPER peptide. Interactions between the light chain of 10E8 and the double-stapled peptide also closely mimicked the interactions observed with the native gp41 MPER peptide (**Supplementary Table 3**). Finally, structural superposition of the 10E8 Fab–SAH-MPER$_{(662–683KKK)}$(B,q) and 4E10 Fab–SAH-MPER$_{(671–683KKK)}$(q) complexes highlights the capacity of hydrocarbon-stapled antigens bearing the 671–683 motif to be differentially engaged by two distinct Fabs, each with potent and broadly neutralizing anti–HIV-1 activity (**Fig. 7c**)[10,12].

DISCUSSION

The development of a safe and effective HIV-1 vaccine represents one of the most formidable scientific challenges of our time and remains the potential game-changer for curbing the global HIV-1 epidemic. The HIV-1 envelope glycoprotein represents the main target for a humoral immune response, yet the emergence of broadly neutralizing antibodies during natural infection occurs only after one or more years of infection, owing to a series of viral immune-evasion maneuvers[50–52]. Underlying the many 'faces' of the HIV-1 envelope are critical functional intermediates whose structures, although shielded or only transiently exposed, provide a possible blueprint for antigen design. One such motif is the MPER domain, which is the physiologic target for a few broadly neutralizing antibodies. The structures of these antibody–MPER complexes, in addition to their non-neutralizing counterparts, have provided tremendous insight into exactly what three-dimensional peptide-encoded configuration may be required to guide an effective anti–HIV-1 immune response[53,54]. How to recapitulate and then stabilize the correct essential structure(s) in order to create a relatively homogeneous candidate immunogen capable of eliciting a safe, broad and effective immune response has remained elusive.

The helical structure of the MPER domain when bound to distinct broadly neutralizing antibodies, such as 4E10 (ref. 9) and the recently identified 10E8 (10), suggests that structurally constrained peptides may provide a highly desirable template for candidate immunogen design. Seminal work in this area has led to both the identification of key residues for 4E10 engagement of a minimal essential helical MPER motif[11] and the demonstration that peptide constraint through the installation of thioether, lactam or triazole cross-links, or helix-promoting non-natural amino acids, could reinforce its structure and increase antibody binding affinity[18,33,55]. Structural analysis of the full-length MPER domain in a lipid context previously revealed a helix-kink-helix conformation, with α-helicity extending to the N terminus just after a bend induced at F673 (ref. 17). We viewed this bipartite structure as an ideal opportunity to increase the immunogenic surface compared to that of the minimal 4E10-binding epitope (671–683) by reinforcing both helical segments through installation of double constraints. We chose the all-hydrocarbon cross-link afforded by olefin metathesis of installed non-natural amino acids bearing olefin tethers[56] because of the unique proteolytic stability conferred and the protease resistance of the hydrocarbon staple itself[34]. Guided by competitive 4E10 binding activity, we determined that antibody engagement of the C-terminal region of the MPER domain is exquisitely sensitive to the site of staple insertion. Indeed, a single *i*, *i* + 3 staple flanking the LW (679-680) sequence, previously shown to be critical for antibody interaction, yielded up to 60-fold enhancement in competitive 4E10 binding activity compared to the unmodified MPER peptide (**Figs. 1c** and **6a**). The 10E8 antibody engages both N- and C-terminal regions of the MPER domain and, in contrast to the 4E10 Fab, 10E8 was sensitive to the positioning of the N-terminal staple. These structure-activity relationship data highlight the capacity of staple scanning to uncover optimal sites for staple incorporation and antigenic structure stabilization.

Our *i*, *i* + 3 stapling efforts and the synthetic challenges encountered in generating double-stapled (*i*, *i* + 4), (*i*, *i* + 3) constructs with the traditional *S*5 non-natural residue prompted us to develop optimized *i*, *i* + 3 stapling chemistry that replaced *S*5 with *R*3 at the N-terminal stapling position. This intervention led to facile production of single- and double-stapled MPER peptides incorporating *i*, *i* + 3 cross-links, with reaction conditions and yields matching those of traditional *i*, *i* + 4 stapling with *S*5 residues. Double-stapled constructs demonstrated nanomolar competitive binding affinity toward 4E10 and 10E8, with the best binder also manifesting 70-fold enhancement in proteolytic stability compared to the corresponding unstapled MPER peptide. This combination of structural stabilization and protease resistance afforded by hydrocarbon double-stapling may represent a highly desirable outcome for candidate immunogen development.

Structural analyses of SAH-MPER peptides in complex with 4E10 and 10E8 Fabs demonstrated the capacity of hydrocarbon stapling to recapitulate native antigenic peptide structures for two distinct broadly neutralizing anti-HIV-1 antibodies while preserving the critical peptide-binding interface by positioning the *i*, *i* + 3 cross-link on the noninteracting surface. The identification of an incorporated phosphate ion near the antigen-binding region of 4E10 revealed a potential phospholipid-binding site. Crystal structures of another broadly neutralizing anti–HIV-1 antibody, 2F5, in complex with the MPER domain identified a putative anionic lipid-binding site, on the basis of incorporation of a sulfate ion at the base of the CDR-H3 loop at high sulfate concentrations[57]. The binding mode and affinity by which diverse broadly neutralizing antibodies engage the lipid membrane may have important implications for candidate immunogen design and efficacy, and immunologic side effects[38,39,43,57]. By incorporating a phosphate tether into the SAH-MPER design, we effectively accessed the identified phosphate-binding region on 4E10. Indeed, as structured templates, hydrocarbon-stapled peptides are amenable to derivatization to incorporate ancillary antibody-binding determinants, and they also reinforce unique architectures, such as the helix-kink-helix MPER motif. Thus, hydrocarbon stapling may serve as a useful addition to the arsenal of approaches aimed at fashioning just the right peptidic structure to elicit broadly neutralizing antibodies for HIV-1 and perhaps other vaccine targets.

METHODS

Methods and any associated references are available in the online version of the paper.

Accession codes. Atomic coordinates and structure factors have been deposited in the Protein Data Bank under accession codes 4NHC (4E10 Fab–SAH-MPER$_{(671–683KKK)}$(q)), 4NGH (4E10 Fab–SAH-MPER$_{(671–683KKK)}$(q)pSer) and 4U6G (10E8 Fab–SAH-MPER$_{(662–683KKK)}$(B,q)).

Note: Any Supplementary Information and Source Data files are available in the online version of the paper.

ACKNOWLEDGMENTS

We thank E. Smith for graphics assistance, D. Ekiert and E. Reinherz for insightful discussions, M. Connors (National Institute of Allergy and Infectious Diseases) for his generosity in providing us with a sample of 10E8 antibody and Y. Yang and P. Acharya for technical support. We are grateful to the US National Institutes of Health (NIH) AIDS Reagent Program for providing us with 4E10 and 10E8 antibodies. This work was supported by NIH grants 1R01 AI084102 (L.D.W.) and R01 AI084817 (I.A.W.); Scripps Center for HIV/AIDS Vaccine Immunology and Immunogen Discovery (CHAVI-ID) grant UM1 AI100663 (I.A.W.); the International AIDS Vaccine Initiative (IAVI) Neutralizing Antibody Center, IAVI Collaboration for AIDS Vaccine Discovery; the Bill and Melinda Gates Foundation; and the Intramural Research Program of the Vaccine Research Center, National Institute of Allergy and Infectious Diseases (NIAID), NIH. Use of the 22-ID and 23-ID sectors at Advanced Photon Source was supported by the US Department of Energy, Office of Science, Office of Basic Energy Sciences, under contract nos. W-31-109-Eng-39 and DE-AC02-06CH11357.

AUTHOR CONTRIBUTIONS

G.H.B. and L.D.W. designed, synthesized and characterized SAH-MPER peptides and conducted the antibody binding, peptide proteolysis and MS analyses; A.I. and I.A.W. performed the structural studies of the 4E10 Fab–SAH-MPER complexes; and G.O. and P.D.K. conducted the structural analysis of the 10E8 Fab–SAH-MPER complex. L.D.W. wrote the manuscript with contributions from all authors.

COMPETING FINANCIAL INTERESTS

The authors declare competing financial interests: details are available in the online version of the paper.

1. Fauci, A.S. *et al.* HIV vaccine research: the way forward. *Science* **321**, 530–532 (2008).
2. Rits-Volloch, S., Frey, G., Harrison, S.C. & Chen, B. Restraining the conformation of HIV-1 gp120 by removing a flexible loop. *EMBO J.* **25**, 5026–5035 (2006).
3. Matthews, T.J. *et al.* Interaction between the human T-cell lymphotropic virus type IIIB envelope glycoprotein gp120 and the surface antigen CD4: role of carbohydrate in binding and cell fusion. *Proc. Natl. Acad. Sci USA* **84**, 5424–5428 (1987).
4. Xiao, L. *et al.* CCR5 coreceptor usage of non-syncytium-inducing primary HIV-1 is independent of phylogenetically distinct global HIV-1 isolates: delineation of consensus motif in the V3 domain that predicts CCR-5 usage. *Virology* **240**, 83–92 (1998).
5. Buzon, V. *et al.* Crystal structure of HIV-1 gp41 including both fusion peptide and membrane proximal external regions. *PLoS Pathog.* **6**, e1000880 (2010).
6. Chan, D.C., Fass, D., Berger, J.M. & Kim, P.S. Core structure of gp41 from the HIV envelope glycoprotein. *Cell* **89**, 263–273 (1997).
7. Muster, T. *et al.* A conserved neutralizing epitope on gp41 of human immunodeficiency virus type 1. *J. Virol.* **67**, 6642–6647 (1993).
8. Zwick, M.B. *et al.* Broadly neutralizing antibodies targeted to the membrane-proximal external region of human immunodeficiency virus type 1 glycoprotein gp41. *J. Virol.* **75**, 10892–10905 (2001).
9. Stiegler, G. *et al.* A potent cross-clade neutralizing human monoclonal antibody against a novel epitope on gp41 of human immunodeficiency virus type 1. *AIDS Res. Hum. Retroviruses* **17**, 1757–1765 (2001).
10. Huang, J. *et al.* Broad and potent neutralization of HIV-1 by a gp41-specific human antibody. *Nature* **491**, 406–412 (2012).
11. Brunel, F.M. *et al.* Structure-function analysis of the epitope for 4E10, a broadly neutralizing human immunodeficiency virus type 1 antibody. *J. Virol.* **80**, 1680–1687 (2006).
12. Cardoso, R.M. *et al.* Broadly neutralizing anti-HIV antibody 4E10 recognizes a helical conformation of a highly conserved fusion-associated motif in gp41. *Immunity* **22**, 163–173 (2005).
13. Coutant, J. *et al.* Both lipid environment and pH are critical for determining physiological solution structure of 3-D-conserved epitopes of the HIV-1 gp41-MPER peptide P1. *FASEB J.* **22**, 4338–4351 (2008).
14. Huarte, N., Lorizate, M., Kunert, R. & Nieva, J.L. Lipid modulation of membrane-bound epitope recognition and blocking by HIV-1 neutralizing antibodies. *FEBS Lett.* **582**, 3798–3804 (2008).
15. Montero, M., van Houten, N.E., Wang, X. & Scott, J.K. The membrane-proximal external region of the human immunodeficiency virus type 1 envelope: dominant site of antibody neutralization and target for vaccine design. *Microbiol. Mol. Biol. Rev.* **72**, 54–84 (2008).
16. Ofek, G. *et al.* Structure and mechanistic analysis of the anti-human immunodeficiency virus type 1 antibody 2F5 in complex with its gp41 epitope. *J. Virol.* **78**, 10724–10737 (2004).
17. Sun, Z.Y. *et al.* HIV-1 broadly neutralizing antibody extracts its epitope from a kinked gp41 ectodomain region on the viral membrane. *Immunity* **28**, 52–63 (2008).
18. Cardoso, R.M. *et al.* Structural basis of enhanced binding of extended and helically constrained peptide epitopes of the broadly neutralizing HIV-1 antibody 4E10. *J. Mol. Biol.* **365**, 1533–1544 (2007).
19. Penn-Nicholson, A. *et al.* Assessment of antibody responses against gp41 in HIV-1-infected patients using soluble gp41 fusion proteins and peptides derived from M group consensus envelope. *Virology* **372**, 442–456 (2008).
20. Scherer, E.M., Leaman, D.P., Zwick, M.B., McMichael, A.J. & Burton, D.R. Aromatic residues at the edge of the antibody combining site facilitate viral glycoprotein recognition through membrane interactions. *Proc. Natl. Acad. Sci. USA* **107**, 1529–1534 (2010).
21. Ofek, G. *et al.* Elicitation of structure-specific antibodies by epitope scaffolds. *Proc. Natl. Acad. Sci. USA* **107**, 17880–17887 (2010).

22. Guenaga, J. *et al.* Heterologous epitope-scaffold prime:boosting immuno-focuses B cell responses to the HIV-1 gp41 2F5 neutralization determinant. *PLoS ONE* **6**, e16074 (2011).
23. Correia, B.E. *et al.* Computational design of epitope-scaffolds allows induction of antibodies specific for a poorly immunogenic HIV vaccine epitope. *Structure* **18**, 1116–1126 (2010).
24. Correia, B.E. *et al.* Computational protein design using flexible backbone remodeling and resurfacing: case studies in structure-based antigen design. *J. Mol. Biol.* **405**, 284–297 (2011).
25. Stanfield, R.L. *et al.* Structure-based design of a protein immunogen that displays an HIV-1 gp41 neutralizing epitope. *J. Mol. Biol.* **414**, 460–476 (2011).
26. Yi, G. *et al.* Chimeric rhinoviruses displaying MPER epitopes elicit anti-HIV neutralizing responses. *PLoS ONE* **8**, e72205 (2013).
27. Dawood, R. *et al.* Generation of HIV-1 potent and broad neutralizing antibodies by immunization with postfusion HR1/HR2 complex. *AIDS* **27**, 717–730 (2013).
28. Wahome, N. *et al.* Conformation-specific display of 4E10 and 2F5 epitopes on self-assembling protein nanoparticles as a potential HIV vaccine. *Chem. Biol. Drug Des.* **80**, 349–357 (2012).
29. Black, M., Trent, A., Tirrell, M. & Olive, C. Advances in the design and delivery of peptide subunit vaccines with a focus on toll-like receptor agonists. *Expert Rev. Vaccines* **9**, 157–173 (2010).
30. Purcell, A.W., McCluskey, J. & Rossjohn, J. More than one reason to rethink the use of peptides in vaccine design. *Nat. Rev. Drug Discov.* **6**, 404–414 (2007).
31. Slingluff, C.L. Jr. The present and future of peptide vaccines for cancer: single or multiple, long or short, alone or in combination? *Cancer J.* **17**, 343–350 (2011).
32. Ho, J. *et al.* Conformational constraints imposed on a pan-neutralizing HIV-1 antibody epitope result in increased antigenicity but not neutralizing response. *Vaccine* **23**, 1559–1573 (2005).
33. Ingale, S., Gach, J.S., Zwick, M.B. & Dawson, P.E. Synthesis and analysis of the membrane proximal external region epitopes of HIV-1. *J. Pept. Sci.* **16**, 716–722 (2010).
34. Bird, G.H. *et al.* Hydrocarbon double-stapling remedies the proteolytic instability of a lengthy peptide therapeutic. *Proc. Natl. Acad. Sci. USA* **107**, 14093–14098 (2010).
35. Leaman, D.P. & Zwick, M.B. Increased functional stability and homogeneity of viral envelope spikes through directed evolution. *PLoS Pathog.* **9**, e1003184 (2013).
36. Zolla-Pazner, S. A critical question for HIV vaccine development: which antibodies to induce? *Science* **345**, 167–168 (2014).
37. Scherer, E.M., Zwick, M.B., Teyton, L. & Burton, D.R. Difficulties in eliciting broadly neutralizing anti-HIV antibodies are not explained by cardiolipin autoreactivity. *AIDS* **21**, 2131–2139 (2007).
38. Matyas, G.R. *et al.* Neutralizing antibodies induced by liposomal HIV-1 glycoprotein 41 peptide simultaneously bind to both the 2F5 or 4E10 epitope and lipid epitopes. *AIDS* **23**, 2069–2077 (2009).
39. Matyas, G.R., Beck, Z., Karasawas, N. & Alving, C.R. Lipid binding properties of 4E10, 2175, and WR304 monoclonal antibodies that neutralize HIV-1. *Biochim. Biophys. Acta* **1788**, 660–665 (2009).
40. Maeso, R. *et al.* Interaction of anti-HIV type 1 antibody 2F5 with phospholipid bilayers and its relevance for the mechanism of virus neutralization. *AIDS Res. Hum. Retroviruses* **27**, 863–876 (2011).
41. Haynes, B.F. *et al.* Cardiolipin polyspecific autoreactivity in two broadly neutralizing HIV-1 antibodies. *Science* **308**, 1906–1908 (2005).
42. Alam, S.M. *et al.* The role of antibody polyspecificity and lipid reactivity in binding of broadly neutralizing anti-HIV-1 envelope human monoclonal antibodies 2F5 and 4E10 to glycoprotein 41 membrane proximal envelope epitopes. *J. Immunol.* **178**, 4424–4435 (2007).
43. Chen, J. *et al.* Mechanism of HIV-1 neutralization by antibodies targeting a membrane-proximal region of gp41. *J. Virol.* **88**, 1249–1258 (2014).
44. Bernal, F. *et al.* A stapled p53 helix overcomes HDMX-mediated suppression of p53. *Cancer Cell* **18**, 411–422 (2010).
45. LaBelle, J.L. *et al.* A stapled BIM peptide overcomes apoptotic resistance in hematologic cancers. *J. Clin. Invest.* **122**, 2018–2031 (2012).
46. Takada, K. *et al.* Targeted disruption of the BCL9/β-catenin complex inhibits oncogenic Wnt signaling. *Sci. Transl. Med.* **4**, 148ra117 (2012).
47. Walensky, L.D. *et al.* Activation of apoptosis *in vivo* by a hydrocarbon-stapled BH3 helix. *Science* **305**, 1466–1470 (2004).
48. Kim, Y.W., Kutchukian, P.S. & Verdine, G.L. Introduction of all-hydrocarbon *i,i*+3 staples into α-helices via ring-closing olefin metathesis. *Org. Lett.* **12**, 3046–3049 (2010).
49. Finton, K.A. *et al.* Autoreactivity and exceptional CDR plasticity (but not unusual polyspecificity) hinder elicitation of the anti-HIV antibody 4E10. *PLoS Pathog.* **9**, e1003639 (2013).
50. Hraber, P. *et al.* Prevalence of broadly neutralizing antibody responses during chronic HIV-1 infection. *AIDS* **28**, 163–169 (2014).
51. Liao, H.X. *et al.* Co-evolution of a broadly neutralizing HIV-1 antibody and founder virus. *Nature* **496**, 469–476 (2013).
52. Locci, M. *et al.* Human circulating PD-1^{+}CXCR3^{-}CXCR5^{+} memory Tfh cells are highly functional and correlate with broadly neutralizing HIV antibody responses. *Immunity* **39**, 758–769 (2013).
53. Frey, G. *et al.* Distinct conformational states of HIV-1 gp41 are recognized by neutralizing and non-neutralizing antibodies. *Nat. Struct. Mol. Biol.* **17**, 1486–1491 (2010).
54. Frey, G. *et al.* A fusion-intermediate state of HIV-1 gp41 targeted by broadly neutralizing antibodies. *Proc. Natl. Acad. Sci. USA* **105**, 3739–3744 (2008).
55. Ingale, S. & Dawson, P.E. On resin side-chain cyclization of complex peptides using CuAAC. *Org. Lett.* **13**, 2822–2825 (2011).
56. Schafmeister, C., Po, J. & Verdine, G. An all-hydrocarbon cross-linking system for enhancing the helicity and metabolic stability of peptides. *J. Am. Chem. Soc.* **122**, 5891–5892 (2000).
57. Julien, J.P., Bryson, S., Nieva, J.L. & Pai, E.F. Structural details of HIV-1 recognition by the broadly neutralizing monoclonal antibody 2F5: epitope conformation, antigen-recognition loop mobility, and anion-binding site. *J. Mol. Biol.* **384**, 377–392 (2008).

ONLINE METHODS

Peptide synthesis and characterization. MPER and SAH-MPER peptides were synthesized, purified, quantified, and subjected to *in vitro* proteolysis testing as previously described[34,58]. Peptides were produced on an Apex 396 (AAPPTEC) automated peptide synthesizer with Rink amide AM LL resin (EMD Biosciences, 0.2 mmol per g resin), at 20-μmol scale. To accomplish single *i*, *i* + 3 stapling with *S5* residues, prolonged reaction time at elevated temperature (10 h, refluxing dichloroethane) was required to match the yields of traditional *i*, *i* + 4 stapling (4 h, room temperature). Protease reaction samples contained 5 μL peptide in DMSO (1 mM stock) and 195 μL of buffer composed of 50 mM Tris-HCl, pH 7.4, 2 mM $CaCl_2$, and chymotrypsin (0.5 ng/μL). Chymotryptic peptide fragments were analyzed by LC/MS (Agilent 1200).

Competitive 4E10 ELISA binding assay. A competitive enzyme-linked immunosorbent assay (ELISA) was used to determine IC_{50} values for SAH-MPER engagement of the 10E8 (ref. 9) and 4E10 (ref. 10) antibodies. The following antibodies were obtained through the NIH AIDS Reagent Program, Division of AIDS, NIAID, NIH (https://www.aidsreagent.org/): HIV-1 gp41 monoclonal antibody 4E10 (cat. no. 10091) from H. Katinger and HIV-1 anti-gp41 monoclonal antibody 10E8 (cat. no. 12294) from M. Connors. Microwells were coated overnight at 4 °C with 50 μl of 0.1 M $NaHCO_3$, pH 8.0, containing neutravidin (4 μg per ml). Plates were washed four times with an automated plate washer (Bio-Tek, ELX-50) with phosphate-buffered saline containing 0.05% Tween-20 (PBST) and blocked with 4% bovine serum albumin (BSA) in PBST (filled to top of wells) for 45 min at 37 °C. Next, a mixture of biotin–PEG_2–antigen (ELDKWASLWNWFNITNWLWYIK for the 4E10 assay or RRRNEQELLELDKWASLWNWFDITNWLWYIRRRR[10] for the 10E8 assay) (20 nM), 4E10 or 10E8 IgG (0.2 nM), and the competing SAH-MPER peptide (two-fold serial dilution from 2 μM to 4 nM across ten columns) in PBST with 1% BSA (PBST-BSA), was incubated (125 μL total volume) in a separate 96-well plate at 37 °C for 2 h. Controls included wells that lacked SAH-MPER competitor or 4E10 or 10E8 IgG. After washing the blocked neutravidin plate, 100 μL of the binding mixture was added for a 1-h incubation at 37 °C; this was followed by plate washing and the addition of a 1:5,000 dilution of goat anti-human IgG for 10E8 or IgG F(ab′)$_2$ for 4E10 peroxidase conjugate (Pierce) in PBST-BSA. After incubation at room temperature for 40 min, the wells were washed five times with PBST and developed by addition of 50 μl of tetramethylbenzidine (TMB) solution at room temperature. Wells containing the TMB solution were quenched after approximately 10 min by addition of 50 μl of H_2SO_4 (2 M), and absorbance at 450 nm was read on a Spectramax microplate reader (Molecular Devices). Experiments were performed in triplicate and repeated at least twice. IC_{50} values for SAH-MPER competition were calculated by nonlinear regression analysis with Prism software (GraphPad).

4E10 Fab purification and crystallization of 4E10 Fab–SAH-MPER$_{(671–683KKK)}$ complexes. 4E10 IgG1(κ) expressed in recombinant Chinese hamster ovary cells (CHO) was purchased from Polymun Scientific Immunbiologische Forschung GmbH by the International AIDS Vaccine Initiative (IAVI). The 4E10 antigen-binding fragment Fab was obtained by papain digestion and purified to homogeneity as described previously[12]. The 4E10 Fab concentrated to ~10 mg/ml in 20 mM sodium acetate, pH 5.5, was mixed with the SAH-MPER$_{(671–683KKK)}$(q) (Ac-NWFNITNZLWXIK-KKK, where Z is *R*3 and X is *S*5) in a 1:4 protein/peptide molar ratio and incubated overnight at 4 °C before crystallization trials were set up. The IAVI–JCSG–TSRI high-throughput CrystalMation system (Rigaku) was initially used to obtain crystallization conditions for the Fab–SAH-MPER$_{(671–683KKK)}$(q) complex. Very thin, long needles (5–10 μm in diameter) appeared in 2–3 weeks in drops containing 4E10 Fab–SAH-MPER$_{(671–683KKK)}$(q) and reservoir solution (50:50) equilibrated against 0.2 M sodium chloride, 0.1 M Na-K phosphate, pH 6.2, and 50% PEG 200. Micro- and macroseeding techniques with the reservoir solution were used to improve crystal size. The crystals were cryoprotected in mother-liquor solutions containing ~60% PEG 200.

The 4E10 Fab stock mixed with SAH-MPER$_{(671–683KKK)}$(q)pSer (Ac-NWFNITNZLWXI*KKK, where Z is *R*3, X is *S*5 and * is Dab-Gly-pSer) in a 1:5 molar ratio was incubated overnight at 4 °C for complex formation. The initial screening trials lead to identification of several crystallization conditions that produced extremely small crystals. One of the conditions lacking PO_4 ions was then used for further crystal optimization. Briefly, tiny needle crystals, grown by mixing equal amounts of 4E10 Fab–SAH-MPER$_{(671–683KKK)}$(q)pSer with reservoir solution (20% PEG 2000 and 0.1 M Tris, pH 7.0), were crushed with a Hampton Seeding bead and then seeded into a JCSG Top 96 screen (http://www.jcsg.org/top96). Long (~200–300 μm), thick (~60–70 μm) needle-like crystals grew from a mixture of equal amounts of complex and reservoir solution (0.2 M $MgCl_2$, 0.1 M MES, pH 5.5, and 40% PEG 400) and 20% of the aforementioned seeding stock in the final drop. The crystals were cryoprotected before data collection in mother-liquor solution containing approximately 46% PEG 400.

4E10 data collection, structure determination and refinement. The X-ray diffraction data for 4E10 Fab–SAH-MPER$_{(671–683KKK)}$(q) were collected at 110 K on a MARMosaic 300 detector with synchrotron radiation (λ = 1.03317 Å) at the Advanced Photon Source (APS) 23ID-D beamline from crystals of ~40 μm in diameter that diffracted to approximately 2.9-Å resolution. To increase completeness in the high-resolution shell, X-ray data sets from two crystals were indexed and scaled together with HKL2000 (ref. 59). The diffraction data were indexed in space group $P6_122$, as suggested by pointless[60], xprep[61] and Phenix-Xtriage[62]. Molecular replacement was performed with Phaser[63], which led to one Fab–peptide complex per asymmetric unit with rotation- and translation-function Z scores of 10.6 and 42.8, respectively, and a log-likelihood gain of 3,655. The initial positions of the models were optimized by rigid-body refinement with Phenix[64]. Rebuilding of the model was performed in Coot[65]. Refinement was accomplished with Phenix with secondary-structure restraints coupled with the refinement of individual atomic coordinates with gradient-driven (LBFGS) minimization and torsion angle–simulated annealing, occupancy refinement, refinement of individual atomic displacement parameters and TLS refinement. Optimization of X-ray–stereochemistry and X-ray–ADP weights were also performed during refinement cycles. X-ray data quality and refinement statistics are included in **Table 1**. The Ramachandran statistics show 90.9% of the residues in the most-favored regions, 6.6% in the additional allowed regions, and 2.5% in the disallowed regions. PyMOL (http://www.pymol.org/) was used to generate the crystallographic images.

The 4E10 Fab–SAH-MPER$_{(671–683KKK)}$(q)pSer structure was solved from a single-crystal X-ray diffraction data set (2.68-Å resolution) collected at 110 K on a MARMosaic 300 detector at the APS 23ID-B beamline with a radiation wavelength of 1.03330 Å. Although the crystals were obtained from a different mother-liquor composition than that of the 4E10 Fab–SAH-MPER$_{(671–683KKK)}$(q) crystals, the autoindexing suggested the same $P6_122$ space group with similar unit-cell values (**Table 1**). Molecular replacement performed with Phaser[63] with only the Fab residues of the 4E10 Fab–SAH-MPER$_{(671–683KKK)}$(q) complex resulted in one complex per asymmetric unit with model rotation- and translation-function Z scores of 13.3 and 68.2, respectively, and a log-likelihood gain of 4,403. Model building and refinement was performed as for the 4E10 Fab–SAH-MPER$_{(671–68KKK)}$(q) complex except that Cartesian-simulated annealing was used instead. The Ramachandran statistics show 93.8% of the residues in the most-favored regions, 4.7% in the additional allowed regions, and 1.5% in the disallowed regions.

Expression and purification of 10E8 and generation of Fabs. Transient expression of the 10E8 antibody was undertaken in HEK293F cells or Expi293 cells per the manufacturer's instructions (Life Technologies) by cotransfection of equal amounts of the 10E8 heavy- and light-chain plasmids, as previously described[66]. 10E8 IgG was purified by capture with Protein A Sepharose (Pierce) and subsequent elution in low pH (Pierce) with adjustment of eluate pH with Tris-Cl, pH 8.0. The 10E8 Fab was prepared with endoproteinase Lys-C (Roche) digestion, as previously described[66]. The LysC protease was added at concentrations of 1:1,000 to 1:10,000, and the digestion was undertaken at 37 °C for 4–6 h. Digestion reactions were stopped with protease-inhibitor tablets (Roche), and cleaved products were run over a Protein A column to segregate the Fc fragment. 10E8 Fab was then subjected to cation-exchange (Mono S) and size-exclusion (S200) chromatography; this was followed by dialysis of peak fractions into 150 mM NaCl, 2.5 mM Tris, pH 7.5, and 0.02% NaN_3.

10E8 crystallization, structure determination, and structural analysis. Purified 10E8 Fab in complex with SAH-MPER$_{(662–683KKK)}$(B,q) was set up in crystallization screens with a Honeybee 963 robot. 576 initial conditions adapted from the commercially available Hampton (Hampton Research), Precipitant Synergy

doi:10.1038/nsmb.2922

(Emerald Biosystems), and Wizard (Emerald Biosystems) crystallization screens were used to set up vapor-diffusion sitting-drop crystallizations at 20 °C. Crystal trays were imaged with the use of a Rockimager (Formulatrix), and crystal hits were optimized manually. Crystals of the 10E8 Fab in complex with SAH-MPER$_{(662–683KKK)}$(B,q) were obtained in a crystallization condition comprising 32% isopropanol, 7.5% PEG 8000, and 0.1 M imidazole, pH 6.5. Diffraction to 4.15-Å resolution was obtained in a cryoprotectant composed of mother liquor supplemented with 50% sucrose and excess peptide. Diffraction data were collected at SER CAT ID-22 beamline of the Advanced Photon Source with a radiation wavelength of 1.0000 Å and processed with HKL-2000 (ref. 59). The structure was solved with molecular replacement with Phaser[63], with the high-resolution structure of 10E8 Fab in complex with gp41 MPER peptide (PDB 4G6F) serving as the search model. Refinement was undertaken with Phenix[67], with PDB 4G6F as a reference model, with iterative model building in Coot[68]. Structures were validated with MolProbity[69] and then analyzed with PISA for buried surface areas and residues[70] and lsqkab for r.m.s.-deviation alignments (CCP4 package)[71]. The Ramachandran statistics show 96.56% of the residues in the most-favored regions, 2.77% in the additional allowed regions, and 0.67% in the disallowed regions.

58. Bird, G.H., Bernal, F., Pitter, K. & Walensky, L.D. Synthesis and biophysical characterization of stabilized α-helices of BCL-2 domains. *Methods Enzymol.* **446**, 369–386 (2008).
59. Otwinowski, Z. & Minor, W. Processing of X-ray diffraction data collected in oscillation mode. *Methods Enzymol.* **276**, 307–326 (1997).
60. Evans, P. Scaling and assessment of data quality. *Acta Crystallogr. D Biol. Crystallogr.* **62**, 72–82 (2006).
61. Sheldrick, G.M. A short history of SHELX. *Acta Crystallogr. A* **64**, 112–122 (2008).
62. Zwart, P.H., Grosse-Kunsteleve, R.W. & Adams, P.D. Characterization of X-ray data sets. *CCP4 Newslett.* **42**, 1–10 (2005).
63. McCoy, A.J. *et al.* Phaser crystallographic software. *J. Appl. Crystallogr.* **40**, 658–674 (2007).
64. Adams, P.D. *et al.* PHENIX: a comprehensive Python-based system for macromolecular structure solution. *Acta Crystallogr. D Biol. Crystallogr.* **66**, 213–221 (2010).
65. Emsley, P., Lohkamp, B., Scott, W.G. & Cowtan, K. Features and development of Coot. *Acta Crystallogr. D Biol. Crystallogr.* **66**, 486–501 (2010).
66. Huang, J. *et al.* Broad and potent neutralization of HIV-1 by a gp41-specific human antibody. *Nature* **491**, 406–412 (2012).
67. Adams, P.D. *et al.* PHENIX: building new software for automated crystallographic structure determination. *Acta Crystallogr. D Biol. Crystallogr.* **58**, 1948–1954 (2002).
68. Emsley, P. & Cowtan, K. Coot: model-building tools for molecular graphics. *Acta Crystallogr. D Biol. Crystallogr.* **60**, 2126–2132 (2004).
69. Davis, I.W. *et al.* MolProbity: all-atom contacts and structure validation for proteins and nucleic acids. *Nucleic Acids Res.* **35**, W375–W383 (2007).
70. Krissinel, E. & Henrick, K. Inference of macromolecular assemblies from crystalline state. *J. Mol. Biol.* **372**, 774–797 (2007).
71. Winn, M.D. *et al.* Overview of the CCP4 suite and current developments. *Acta Crystallogr. D Biol. Crystallogr.* **67**, 235–242 (2011).